Theor Chem Acc (1997) 97:317–323

Theoretical
Chemistry Accounts

Variational transition state theory without the minimum-energy path

Jordi Villa*,, Donald G. Truhlar**

Department of Chemistry and Supercomputer Institute, University of Minnesota, Minneapolis, MN 55455-0431, USA

Received: 22 January 1997 / Accepted: 11 March 1997

Abstract. In this paper we propose a method for carrying out variational transition state theory calculations without first obtaining a converged minimum-energy path (MEP). We illustrate the method in two ways, first of all by employing an unconverged MEP and secondly by using a dynamically optimized distinguished reaction path. Preliminary tests of the algorithm for the reactions $OH + H_2 \rightarrow H_2O + H$ and $C_2H_5 \rightarrow C_2H_4 + H$ are very encouraging.

Key words: Variational transition state theory – Reaction path – Optimization of dividing surface – Dynamics – Free energy of activation

1 Introduction

Variational transition state theory (VTST) provides a powerful computational tool for the study of chemical reaction rates, and it has been applied successfully to a variety of reactions in both the gaseous and condensed phases. Several reviews are available [1–8]. The ultimate justification for the variational aspect of VTST is the theorem, strictly valid only in classical mechanics, that the one-way reactive flux through a dividing surface separating reactants and products provides an upper bound to the local-equilibrium reaction rate [9–12]. It is well known that the statistical mechanical evaluation of the one-way flux coefficient at temperature T through a trial dividing surface, generalized transition state (GT), parameterized by a set of parameters P yields [9–12]

$$k(T) = \frac{\tilde{k}T}{h} K^{\dagger,0} \exp\{-[G^{\mathrm{GT},0}(T,P) - G^{R,0}(T)]/RT\} \quad (1)$$

where $\tilde{k}$ is Boltzmann's constant, h is Planck's constant, $K^{\dagger,0}$ is unity for unimolecular reactions and the reciprocal of the concentration in the standard state for bimolecular reactions, $G^{\mathrm{GT},0}(T,P)$ is the standard-state molar free energy of systems in the dividing surface, $G^{R,0}(T)$ is the standard-state molar free energy of reactants, and R is the gas constant. When the parameter P in Eq. (1) is varied to maximize the free energy of the GT, Eq. (1) becomes the canonical VTST expression for the rate coefficient, usually abbreviated CVTST or CVT. In practice, Eq. (1) is usually multiplied by a transmission coefficient to account for, inter alia, tunneling, nonclassical reflection along the reaction coordinate, and incomplete minimization of the rate coefficient with respect to P, but consideration of such refinements is beyond the scope of the present paper.

We note as critical background for what follows that a system mathematically localized in a dividing surface has one less degree of freedom than an equilibrium species. Thus, for a reactive system with N atoms, a nonlinear GT has 3 translations, 3 rotations, $3N-7$ vibrations, and one degree of freedom orthogonal to the dividing surface. The last-named degree of freedom is traditionally called the reaction coordinate or the "missing" degree of freedom. Both conventional and VTST assume that the missing degree of freedom is locally separable. In classical mechanics, if this degree of freedom is not locally separable, one expects the upper bound to be a poor one due to trajectories recrossing the dividing surface (recrossing and breakdown of the bound can also occur due to global nonseparability, so local separability is a necessary but not a sufficient criterion for the accuracy of the theory). In a quantum mechanical computation, where vibrations are quantized in calculating the free energies, local nonseparability of the reaction coordinate is again expected to make the calculated rate coefficient too high, due now to the quantum mechanical analog of recrossing trajectories. In addition, local nonseparability makes the validity of any approximations (e.g., the harmonic approximation) employed in calculating $G^{\mathrm{GT},0}(T,P)$ quite uncertain, which could cause the calculated rate coefficient to be either too large or too small. In this respect we remind

* Visiting scientist, Fall 1996–Winter 1997

** *Present address*: Departament de Química, Universitat Autònoma de Barcelona, E-08193 Bellaterra, Barcelona, Spain
Correspondence to: D.G. Truhlar

the reader that in a quantum mechanical world, it is more appropriate to visualize the GTs as having a finite width in the direction of the reaction coordinate [8, 13], so nonseparability becomes even more significant.

Almost all practical applications of VTST have used the same prescription for parameterizing the trial surfaces, which are called GTs, and which are the trial variational transition states. This prescription, introduced in 1979 [14–17], is strongly tied to a steepest-descents reaction path. First one calculates the steepest-descents path in isoinertial coordinates (i.e., coordinates scaled to the same reduced mass for all possible directions of motion, e.g., normal coordinates of the saddle point or mass-scaled or mass-weighted Cartesians). Such a steepest-descents path is called the minimum-energy path (MEP) [16, 18–20] or the intrinsic reaction path [21]. One defines a scalar reaction coordinate s as the signed arc length along this path. Then one defines a single trial surface for each value of s such that the trial surface intersects the MEP at s and is locally orthogonal to the path. Since a steepest-descents path, by definition, is locally tangent to the gradient of the potential energy function, this means that the trial dividing surface is, at the point where it intersects the MEP, orthogonal to the gradient. For this set of trial dividing surfaces, the parameter set P reduces to a single scalar variable s. Then $G^{\mathrm{GT},0}(T,s)$ is maximized with respect to s.

Three critical questions arise at this point:

1. Is this set of trial dividing surfaces complete enough to find a variationally best transition state which is good enough to calculate accurate rate coefficients?

2. Is the reaction coordinate separable enough to make recrossing effects small when trial dividing surfaces are defined this way?

3. Are approximate quantized energy levels calculated with practical techniques for such trial dividing surfaces accurate enough to calculate quantitatively accurate rate coefficients in a quantum mechanical world?

These questions have been answered primarily through experience [2, 3, 8, 15, 16, 22–28] by comparing CVT rate constants to accurate quantal ones or to experimental values, and the answers appear to be (1) yes, (2) yes, (3) yes if curvilinear coordinates are used off the MEP and anharmonicity is included. When the harmonic approximation is employed and the vibrations are treated entirely in rectilinear coordinates, the quantized vibrational levels of the generalized transition are less physical, but the theory is still very useful for interpreting experiments and predicting experimental rate coefficients since the errors in the dynamical theory still appear to be much smaller than the typical error attributable to uncertainties in potential energy functions (e.g., an error of 1.4 kcal/mol in the barrier height leads to an error of a factor of 9.4 in the calculated rate coefficient at room temperature, and the errors due to rectilinear vibrational frequencies and neglect of anharmonicity are expected to be smaller than this in most cases). In the present paper we accept the limitations of rectilinear frequencies and the neglect of anharmonicity, but progress is being made in allowing the use of curvilinear coordinates, as discussed elsewhere [29–31] and new practical methods that may be useful for including anharmonicity are available as well [32, 33].

The success of VTST calculations based on searching along the MEP for the best transition state has perhaps overshadowed one of its limitations, namely that it can be expensive to calculate the MEP because small step sizes are required to accurately compute a steepest-descents path [34]. *The main point of the present paper is to present a practical method for carrying out* VTST *calculations without calculating an* MEP. A spin-off benefit of the proposed algorithm is that it can also be used to extract a stable and meaningful CVT free energy of activation from an MEP-based calculation carried out with such large steps sizes that previously available algorithms for calculating this quantity [34, 35] were unstable or inaccurate.

Two other concepts that should be explained as background to the present work are the distinguished-co ordinate reaction path [36–38] which we call the distinguished coordinate path (DCP), and the gradient extremal path (GEP) [38–43]. Both these types of path, while not identical to the MEP, have the advantage that they can be calculated with arbitrarily large step sizes (because they are defined locally and not just in terms of following a path continuously from the saddle point), but in many cases they are expected to be close to, although definitely not on, the MEP. One way to understand the goal of the present work is to note that we have now developed an algorithm that can be used to carry out VTST calculations with data along a DCP, GEP, or incompletely converged MEP, whereas the previous algorithm required one to have data along a well-converged MEP. We will justify the new algorithm, though, in terms of the empirically successful MEP approach, and the approximations we make are such that the new method may well work best when the data points obtained by a DCP, GEP, or large-step-size MEP calculation (or any other similar method) are not too far from the true MEP. We emphasize again though that the previous algorithm was sensitive to even very small deviations of the path points from the true MEP.

A point on a DCP is obtained by distinguishing some internal coordinate as an approximate reaction coordinate, constraining it to some predetermined value, and optimizing the system (i.e., minimizing its energy) with respect to all the other internal coordinates. For example, in the concerted reaction $\mathrm{A} + \mathrm{BC} \rightarrow \mathrm{AB} + \mathrm{C}$, one might distinguish the A—B bond distance as an approximate reaction coordinate on the reactant side of the saddle point and the B—C bond distance as an approximate reaction coordinate on the product side.

A point on a GEP is obtained by finding the location where the gradient direction coincides with the direction of one of the eigenvectors of the hessian. Since the GEP in isoinertial coordinates passes through the reactants, products, and saddle point and is locally tangent to the MEP at those points, it is expected to often lie close to the converged MEP even at finite distances from the stationary points.

2 Theory

We assume that a Taylor series of the potential, valid through quadratic terms, is available for each of a series of points along some reaction path which is not the converged MEP. Specify these points as $k = 1, 2, \ldots, K$. Let x denote a $3N$-dimensional rectilinear isoinertial coordinate system [32, 41], (A rectilinear coordinate system is any coordinate system that can be obtained from atomic cartesians by a linear transformation; this includes normal-mode coordinates and Jacobi coordinates as special cases.) Although the present development is valid for any rectilinear, isoinertial coordinate system, for concreteness we let

$$x_i = (m_i/\mu)^{1/2} R_i, \tag{2}$$

where R_1, R_2, R_3, m_1, m_2, and m_3 are the cartesian coordinates and mass of atom 1, R_4, R_5, R_6, m_4, m_5, and m_6 are the cartesian coordinates and mass of atom 2, etc. Let $\mathbf{x}(k)$ denote the K points where data is available. We will consider trial dividing surfaces that are hyperplanes in $\mathbf{x}$ and that pass through one of the points $\mathbf{x}^L(k)$. Let $\hat{\mathbf{n}}$ denote a unit vector normal to the hyperplane. For each k we optimize the orientation of the dividing surface to maximize the free energy of the generalized state at k. Define the optimized value as

$$G^{\mathrm{OGT},0}(T,k) = \max_{\hat{\mathbf{n}}} G^{\mathrm{GT},0}(T,k,\hat{\mathbf{n}}), \tag{3}$$

where $G^{\mathrm{GT},0}(T,k,\hat{\mathbf{n}})$ is the free energy of the trial transition state passing through point k with orientation normal to $\hat{\mathbf{n}}$. Then the standard-state molar free energy of activation of the variational transition state is calculated by

$$G^{\mathrm{CVT},0} = \max_{k} G^{\mathrm{OGT},0}(T,k,). \tag{4}$$

The new algorithm has two steps: (1) calculation of $G^{\mathrm{GT},0}(T,k,\hat{\mathbf{n}})$, and (2) the maximization of this value with respect to the orientation of the hyperplane, as specified by its unit normal $\hat{\mathbf{n}}$.

Step 1, the calculation of $G^{\mathrm{GT},0}(T,k,\hat{\mathbf{n}})$ proceeds as follows. We assume that the Taylor series of the potential is available though quadratic terms:

$$V(\mathbf{x}) = V_0 + \mathbf{g}^\dagger(k)\mathbf{r} + \frac{1}{2}\mathbf{r}^\dagger \mathbf{F}(k)\mathbf{r}, \tag{5}$$

where

$$\mathbf{r} = \mathbf{x} - \mathbf{x}^L(k) \tag{6}$$

$$V_0 = V[\mathbf{x}^L(k)] \tag{7}$$

$$\mathbf{g}^L(k) = \left.\frac{\partial V}{\partial \mathbf{x}}\right|_{\mathbf{x}=\mathbf{x}^L(k)} = \left.\frac{\partial V}{\partial \mathbf{r}}\right|_{\mathbf{r}=\mathbf{0}}, \tag{8}$$

and

$$\boldsymbol{F}_{ii'}(k) = \left.\frac{\partial^2 V}{\partial x_i \partial x_{i'}}\right|_{\mathbf{x}=\mathbf{x}^L(k)} \tag{9}$$

and † denotes a transpose. Note that $\mathbf{g}^L(k)$ is the gradient and $\mathbf{F}(k)$ is the hessian in the isoinertial coordinate system at $\mathbf{x}^L(k)$, and we have suppressed k in the notation for $\mathbf{r}$, although of course it is a different variable for each k considered.

Consider a particular value of k. First we find the minimum energy in the hyperplane. To accomplish this we define a projected hessian by

$$\mathbf{F}^P(\hat{\mathbf{n}}) = (\mathbf{1} - \hat{\mathbf{n}}\hat{\mathbf{n}}^\dagger)(\mathbf{1} - \mathbf{P}^{\mathrm{RT}})\mathbf{F}(\mathbf{1} - \mathbf{P}^{\mathrm{RT}})(\mathbf{1} - \hat{\mathbf{n}}\hat{\mathbf{n}}^\dagger), \tag{10}$$

where $\mathbf{P}^{\mathrm{RT}}$ projects onto the rotations and translations. This is a generalization of the projector of Miller et al. [45] and reduces to it if we replace $\hat{\mathbf{n}}$ by the gradient direction, which is given by

$$\hat{\mathbf{g}}^L = \mathbf{g}^L / |\mathbf{g}^L|. \tag{11}$$

[Generalizations similar to Eq. (10) have also been used in the context of constrained optimization and constrained reaction paths [46, 47]]. We also define a projected gradient

$$\mathbf{g}^{\mathrm{PL}} = (\mathbf{1} - \hat{\mathbf{n}}\hat{\mathbf{n}}^\dagger)(\mathbf{1} - \mathbf{P}^{\mathrm{RT}})\mathbf{g}^L, \tag{12}$$

where the inclusion of the projector $(\mathbf{1} - \mathbf{P}^{\mathrm{RT}})$ is not mathematically necessary (since the gradient is physically zero in the translational and rotational directions), but it may help reduce rounding errors. Then it is easily seen that the value of $\mathbf{r}$ that minimizes Eq. (5) within the trial hyperplane is

$$\mathbf{r}^M = -(\mathbf{F}^P)^{-1}\mathbf{g}^{\mathrm{PL}}. \tag{13}$$

Note that $\mathbf{g}^{\mathrm{PL}}$ and $\mathbf{r}$ will be zero if $\hat{\mathbf{n}} = \hat{\mathbf{g}}^L$. Finally the minimum value of V is obtained as

$$V^M = V_0 + (\mathbf{g}^{\mathrm{PL}})^\dagger \mathbf{r}^M + 1/2(\mathbf{r}^M)^\dagger \mathbf{F}^P \mathbf{r}^M \tag{14}$$

and the quantized vibrational energies are evaluated by

$$\epsilon(n_1, \ldots, n_{3N-7}) = V^M + \frac{h}{2\pi}\sum_{m=1}^{3N-7} \omega_m \left(n_m + \frac{1}{2}\right), \tag{15}$$

where n_m is the vibrational quantum number of mode m, and

$$\omega_m = (\Lambda_{mm}/\mu)^{1/2}, \tag{16}$$

where Λ_{mm} is an eigenvalue of $\mathbf{F}^P$.

Although the above equations are formally correct, $\mathbf{F}^P$ has seven zero eigenvalues [six if $\mathbf{x}^L(k)$ corresponds to a linear geometry] and hence is singular; thus Eq. (13) cannot be calculated quite so easily. Instead we diagonalize $\mathbf{F}^P$

$$\mathbf{L}^\dagger \mathbf{F}^P \mathbf{L} = \mathbf{\Lambda}, \tag{17}$$

where the columns of $\mathbf{L}$ are the eigenvectors. Then we transform the gradient vector and displacement vector to the eigenvector representation:

$$\mathbf{g}^{\mathrm{EL}} = \mathbf{L}^\dagger \mathbf{g}^{\mathrm{PL}} \tag{18}$$

and

$$\mathbf{r}^{\mathrm{EM}} = \mathbf{L}^\dagger \mathbf{r}^M. \tag{19}$$

In the eigenvector representation, Eq. (13) is replaced by

$$\mathbf{r}^{\mathrm{EM}} = -\mathbf{\Lambda}^{-1}\mathbf{g}^{\mathrm{EL}}. \tag{20}$$

If we order the eigenvalues and eigenvectors so that the zero eigenvalues come last, we can constrain the last seven elements of $\mathbf{r}^{\mathrm{EM}}$ to be equal to zero. This constrains the minimization to conserve the center-of-mass location and the orientation, and it forces the optimized geometry to remain in the trial hypersurface. This is easily accomplished by dropping the last seven rows and columns of $\mathbf{\Lambda}, \mathbf{r}^{\mathrm{EM}}$, and $\mathbf{g}^{\mathrm{EL}}$ in Eq. (20). After solving the resulting $(3N-7)\times(3N-7)$ version of Eq. (20) in this reduced space, we add the last seven elements of $\mathbf{r}^{\mathrm{EM}}$ back as zeros, and we obtain the desired displacement vector in the original mass-scaled Cartesian coordinates by

$$\mathbf{r}^{M} = (\mathbf{L}^{\dagger})^{-1}\mathbf{r}^{\mathrm{EM}}. \tag{21}$$

Now consider step 2, the optimization of the direction of $\hat{\mathbf{n}}$. Step 1 above yields the optimum V^M and the frequencies which we use to calculate $G^{\mathrm{GT},0}(T,k,\hat{\mathbf{n}})$. Call this $G(\hat{\mathbf{n}})$. We find the maximum of $G(\hat{\mathbf{n}})$ iteratively by the conjugate gradient algorithm [48a]. To apply the conjugate gradient algorithm we require the derivatives $\partial G/\partial(\hat{\mathbf{n}})_i$, where $(\hat{\mathbf{n}})_i$ is a component of $\hat{\mathbf{n}}$. These are evaluated by a two-point central difference algorithm. This algorithm produces trial values of $\hat{\mathbf{n}}$ that are not normalized, but this is not a problem since all we require is the direction of $\hat{\mathbf{n}}$, so we normalize $\hat{\mathbf{n}}$.

3 Examples

We will illustrate the theory with three examples. The first case corresponds to a CVT rate calculation at 200 K for the reaction $OH + H_2 \rightarrow H_2O + H$. The other two correspond to the reaction $C_2H_5 \rightarrow C_2H_4 + H$, and since our goal is just to illustrate the theory we consider only $T = 0$ K for this reaction. At zero temperature [17],

$$G^{\mathrm{GT},0}(T=0,k,\hat{\mathbf{n}}) = V_0 + \frac{h}{4\pi}\sum_{m=1}^{3N-7}\omega_m. \tag{22}$$

All calculations were performed with a modified version of the POLYRATE computer program, version 7.0 [49–51]

3.1 Example 1

The first case we consider is the reaction $OH + H_2 \rightarrow H_2O + H$ with the Dunning-Walch-Schatz-Elgersma [52] potential energy function and with an unconverged MEP. The scaling mass is set equal to $m_{\mathrm{OH}}m_{\mathrm{H_2}}/m_{\mathrm{H_3O}} = 1.8$ amu. The MEP was calculated by the Euler method [34, 35] with gradient step size δ and hessian step size 2δ in the range $s = -1.0$ to $+0.3$ a_0. The value of δ is varied from 0.005 to 0.03 a_0. For each value of δ, two calculations are carried out. The first uses our standard algorithms [35, 44, 49] including, e.g., interpolation of the free energies of activation by five-point Langrangian interpolation as the method of searching for the maximum. The second calculation is identical to the first except that V^M and the frequencies are calculated from the Taylor series of Eq. (5), where $\mathbf{x}^L$ is a point on the approximate (unconverged) MEP, by step 1 of the algorithm above, and the orientation of the dividing surface at each hessian point is numerically optimized by step 2 of the algorithm above. Figure 1 compares the calculated CVT rate constant at 200 K as a function of δ for the two procedures. When $\delta = 0.0005\,a_0$, the two procedures give essentially identical results – though the second calculation gives slightly lower values for the CVT rate constant. The figure shows the percentage deviation from that converged value as δ is increased. We see that the original algorithm is very sensitive to lack of convergence of the MEP, with an error of 86% when $\delta = 0.025\,a_0$. For that same value of δ, the new algorithm gives an error of only -10% .

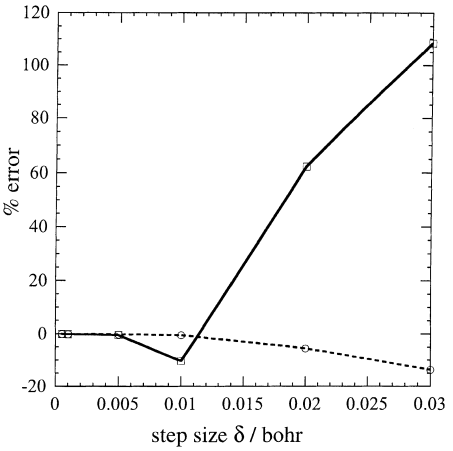

Fig. 1. Percentage error in CVT rate constant for $OH + H_2 \rightarrow H_2O + H$ at 200 K as a function of step size δ used to calculate the reaction path. *Squares* connected by *solid-line segments*: original algorithm. *Circles* connected by *dashed-line segments*: new algorithm

3.2 Example 2

In the second example, we consider the reaction $C_2H_5 \rightarrow C_2H_4 + H$ in the high-pressure limit at the MP2/6-31G(d,p) [53] level of electronic structure with an unconverged MEP. We note for completeness that in the MP2/6-31G(d,p) approximation, the value of $G^{\mathrm{GT},0}(T=0,s)$ is below 38.75 kcal at the reactant geometry where the C—H bond length is 2.069 a_0, increases to 83.42 kcal at the saddle point where the C—H bond distance is 3.523 a_0, and then decreases to 70.68 kcal at the products where the C—H bond length is ∞.

We set the scaling mass μ equal to 1 amu. The MEP was calculated with the Gonzalez-Schlegel mass-weighted internal-coordinates reaction-path algorithm [54] with a reaction-path step size of 0.02 a_0 and a hessian calculated every 0.02 a_0. Again we performed two calculations, one with the original CVT algorithm and one with the new one described above. The results for $G^{\mathrm{GT},0}(T=0,k,s)$ are compared in the vicinity of the saddle point $(s=0)$ in Fig. 2. The calculation with the original algorithm is very noisy, and the one with the new algorithm is smooth. Based on past experience, we attribute the noise to lack of convergence of the MEP.

The new algorithm is much less sensitive to this than the old one.

3.3 Example 3

This example is again based on the reaction $C_2H_5 \rightarrow C_2H_4 + H$ in the high-pressure limit with the MP2/6-31G(d,p) electronic structure level. In this case we compare an MEP-based calculation of $G^{GT,0}(T = 0, s)$ to two calculations based on a DCP, one of them using the hypersurface normal to the gradient and the other one using the algorithm above (steps 1 and 2).

The MEP-based calculation is the same as the calculation in example 2 that applies the new algorithm. This calculation is shown as the open circles connected by a dashed curve. The second and third calculations in Fig. 3 are DCP calculations. With this algorithm, one can take arbitrarily large step sizes, and the points on the DCP and their corresponding free-energy values can be computed in any order since they do not depend on the other points. The distinguished coordinate is taken to be the bond length of the dissociating C—H bond. This internal coordinate is fixed successively at 1.82, 1.84, 1.86, 1.88 and 1.90 Å (or 3.3439, 3.477, 3.515, 3.553, and 3.590 a_0), and we also include the saddle-point geometry (where the C—H distance is 3.523 a_0) as part of the DCP; so $K = 6$. The filled circles connected by a long-dashed line are the results of a DCP calculation using a dividing surface through $\mathbf{x}^L(k)$ and normal to the gradient at $\mathbf{x}^L(k)$. The filled squares connected by a chain curve in Fig. 3 are the results of a DCP calculation using the new algorithm of Sect. 2, in which the orientation of the dividing surface is optimized. The displacement vector $\mathbf{r}^M(k)$ gives the location, relative to $\mathbf{x}^L(k)$, of the point of minimum energy in the optimum dividing surface through $\mathbf{x}^L(k)$.

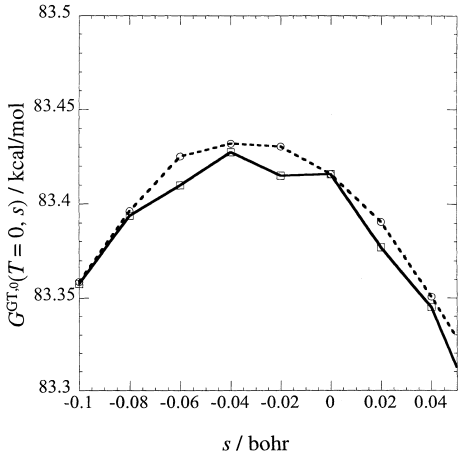

Fig. 2. $G^{GT,0}(T = 0, s)$ for $C_2H_5 \rightarrow C_2H_4 + H$ as a function of position along the reaction path, which is an unconverged minimum-energy path (MEP). Squares connected by *solid-line segments*: original algorithm. *Circles* connected by *dashed-line segments*: new algorithm

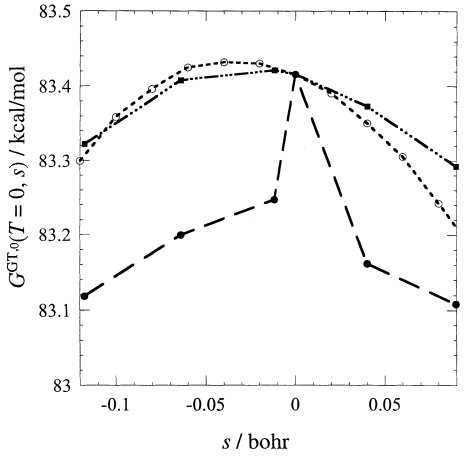

Fig. 3. $G^{GT,0}(T = 0, s)$ for $C_2H_5 \rightarrow C_2H_4 + H$ as a function of position along the MEP. *Circles* connected by *dashed-line segments*: new algorithm with an MEP (same as *dashed curve* in Fig. 2). *Filled circles* connected by *long dashed-line segments*: original algorithm with a distinguished coordinate path (DCP). *Filled squares* connected by *triple-dot-dash line segments*: new algorithm with a DCP

The set of points $\mathbf{x}^L(k)$ defines the DCP, but the analog of the MEP in this method is the set of re-optimized geometries given by

$$\mathbf{x}^M(k) = \mathbf{x}^L(k) + \mathbf{r}^M(k), \tag{23}$$

which may be called the dynamically optimized DCP. In general one would assign an s value by fitting a curve through the collection of these points and calculating the signed distance from the saddle point along this curve. In the present case, we use the simplest possible curve, namely a sequence of straight-line segments connecting the points on the dynamically optimized DCP, including the saddle point. Note that in order to calculate the distance between $\mathbf{x}^M(k)$ and $\mathbf{x}^M(k+1)$, we must first be sure that the orientation of the molecular system is consistent [55]. In the present application this was accomplished in an approximate way by simply orienting each point so that its principal axes of inertia line up with the principal axes at the previous point. The straight line segments are used only to calculate s, yielding values of $-0.117, -0.064, -0.012, 0.040$, and 0.090 a_0 for the five points at which a DCP calculation was carried out (recall that $s = 0.0$ a_0 at the saddle-point location, which is $k = 4$).

The first DCP calculation, namely that obtained with the dividing surface normal to the gradient, has a characteristic dip on both sides of the saddle point. This kind of dip is often found in unconverged MEP calculations, and it has the following origin. If a point on an approximate MEP is too far off the true MEP, the gradient will have a significant component directed toward the MEP in addition to the expected component parallel to the MEP. This is particularly likely to occur if the deviation in geometry has a component along a high-frequency mode, since the potential rapidly becomes steep in those directions. Since the original procedure places the dividing surface normal to the gradient, it effectively moves some of the high-frequency mode into the reaction coordinate, replacing a part of the true reaction coordinate, along which the potential is relatively flat near the saddle point. Similarly a component of the true reaction coordinate is exchanged into the GT dividing

surface, replacing the missing component of the high-frequency mode. As a consequence the calculated frequency of one or more of the modes within the dividing surface is reduced.

The third calculation in Fig. 3 is the DCP calculation improved with the new algorithm above. It is clear that the new algorithm provides a more physical description of the region close to the saddle point. We emphasize that the height of the adiabatic barrier is well described using the new algorithm with the DCP calculation. In particular, if we fit a parabola to the three highest points of the dynamically optimized DCP calculation, we obtain a maximum value of $G^{\mathrm{CVT},0}(T=0)=83.42$ kcal/mol, whereas if we fit a parabola to the three highest points on the MEP curve in Fig. 3, the maximum is $G^{\mathrm{CVT},0}(T=0)=83.43$ kcal/mol. In actual practice, based on results like those in Fig. 3, we might decide to calculate more points in the region close to the maximum of $G^{\mathrm{GT},0}(T=0,s)$ in order to refine the determination of the maximum of the curve and hence calculate a more accurate CVT rate constant. This does not appear necessary in the present case.

4 Discussion

We note that the algorithm as presented here is intentionally very simple. We assume, having found the minimum energy of the trial hyperplane, that the geometry so obtained lies within the trust region for the Taylor series of Eq. (5). Clearly one could improve on this. For example one could evaluate the energy directly at $\mathbf{r}^M$ and compare it to the value calculated from the Taylor expansion at $\mathbf{r}=0$. Or one could consider the algorithm above as the first step in a Newton-Raphson iterative sequence. But either of these alternatives requires additional electronic structure calculations and raises the cost. It seems reasonable to test carefully how far one can proceed with the present simple algorithm and to complicate it only if and when necessary. The results in Sect. 3 show that the new algorithm is quite useful.

We have not addressed the question of tunneling. For ground-state tunneling along the MEP one requires not only the maximum of $G^{\mathrm{GT},0}(T=0,s)$ but also the width and shape of the barrier [19, 20, 35, 44, 56]. As mentioned above, we could convert $\{G^{\mathrm{GT},0}(T=0,k)\}_{k=1}^{K}$ into $G^{\mathrm{GT},0}(T=0,s)$ by fitting the points $\{\mathbf{x}^M(k)\}_{k=1}^{K}$ to a curve through $(3N-7)$-dimensional space and calculating the distance along this curve by numerical integration. In order for the distance along the curve to be meaningful, one will have to be sure that the center of mass and orientation are held constant along the path. The simplest curve (which was used in example 3) is a set of straight lines connecting the points. It would be more accurate to fit the points to a continuous curve. If one does that, one can also attempt to take the derivatives of this curve and calculate its curvature, which allows for a more accurate estimate of tunneling probabilities [35, 49, 57]. It will require careful testing to see if this can be done in a meaningful way without anchoring the path firmly to the MEP. It will be interesting, in future work, to employ DCP (or GEP) calculations with much larger step sizes and develop the procedures for using these for tunneling calculations.

We think that an important use of the algorithm presented here will be to allow the development of improved versions of interpolated VTST (IVTST) [58–61]. In the polyatomic IVTST algorithm that has been proposed so far [59] one calculates free energies for the reactants, products, and saddle point plus one or a few "extra" points on the MEP, and then one interpolates $G^{\mathrm{GT},0}(T,s)$ to the full range of s. However, since the calculation of the MEP requires small steps, we have been restricted to having the extra points very close to the saddle point. It would be much more useful to have extra points half-way or even a quarter of the way down the hill from the saddle point toward reactants and/or products. The present algorithm could be used to obtain such data since the distinguished-coordinate path can be calculated with arbitrarily large step sizes, and the present algorithm allows one to calculate free energies of activation along a distinguished-coordinate path.

5 Conclusion

We have presented an algorithm that allows one to compute VTST rate constants without calculating the MEP with a converged step size. It should allow one to interface electronic structure theory and dynamics in a more efficient way.

Acknowledgements. This work was supported in part by the U.S. Department of Energy, Office of Basic Energy Sciences, and in part by the DGICYT ("Ministerio de Educatión y Ciencia" of Spain) through Project No. PB5-0637.

References

1. Pechukas P (1982) Ber Bunsenges Phys Chem 86:372
2. Truhlar DG, Hase WL, Hynes JT (1983) J Phys Chem 87:2664, 5523(E)
3. Truhlar DG, Garrett BC (1984) Annu Rev Phys Chem 35, 159
4. Laidler KJ (1987) Chemical kinetics, 3rd edn. Harper & Row, New York
5. McKee ML, Page M (1993) Rev Comp Chem 4:35
6. Page ML (1994) Comput Phys Commun 84:115
7. Garrett BC, Schenter GK (1994) Int Rev Phys Chem 13:263
8. Truhlar DG, Garrett BC, Klippenstein SJ (1996) J Phys Chem 100:12771
9. Wigner E (1937) J Chem Phys 5:720
10. Horiuti J (1938) Bull Chem Soc Jpn 13:210
11. Keck JC (1967) Adv Chem Phys 13:85
12. Tucker SC, Truhlar DG (1989) In: Bertran J, Czismadia I, (eds) New theoretical concepts for understanding organic reactivity, Kluwer, Dordrecht, pp 291–346
13. Truhlar DG, Garrett BC (1992) J Phys Chem 96:6515
14. Garrett BC, Truhlar DG (1979) J Chem Phys 70:1593
15. Garrett BC, Truhlar DG (1979) J Phys Chem 83:1052
16. Garrett BC, Truhlar DG (1979) J Phys Chem 83:1079 (1983) 87:4553(E)
17. Garrett BC, Truhlar DG (1979) J Am Chem Soc 101:4534
18. Shavitt I (1968) J Chem Phys 49:4048
19. Truhlar DG, Kuppermann A (1971) J Am Chem Soc 93:1840
20. Truhlar DG, Kuppermann A (1972) J Chem Phys 56:2232
21. Fukui K (1974) In: Daudel R, Pullman B, (eds) The world of quantum chemistry. Reidel, Dordrecht, p 113

22. Truhlar DG, Isaacson AD, Skodje RT, Garrett BC (1982) J Phys Chem 86:2252; (1983) 87:4554(E)
23. Garrett BC, Truhlar DG (1984) J Chem Phys 81:309
24. Garrett BC, Truhlar DG, Schatz GC (1986) J Am Chem Soc 108:2876
25. Garrett BC, Truhlar DG (1991) J Phys Chem 95:10374
26. Melissas VS, Truhlar DG (1993) J Chem Phys 99:3542
27. Mielke SL, Lynch GC, Truhlar DG, Schwenke DW (1994) J Phys Chem 98:8000
28. Mielke SL, Allison TC, Truhlar DG, Schwenke DW (1996) J Phys Chem 100:13588
29. Natanson GA, Garrett BC, Truong TN, Joseph T, Truhlar DG (1991) J Chem Phys 94:7875
30. Jackels CF, Gu Z, Truhlar DG (1995) J Chem Phys 102:3188
31. Nguyen KA, Jackels CF, Truhlar DG (1996) J Chem Phys 104:6491
32. Truhlar DG, Isaacson AD (1991) J Chem Phys 94:357
33. Kuhler KM, Truhlar DG, Isaacson AD (1996) J Chem Phys 104:4664
34. Melissas VS, Truhlar DG, Garrett BC (1992) J Chem Phys 96:5758
35. Truhlar DG, Isaacson AD, Garrett BC (1985) In: Baer M (ed) Theory of chemical reaction dynamics, vol 4. CRC Press, Boca Raton Fla, pp 65–137
36. Rothman MJ, Lohr LL Jr., Ewig CS, van Wazer JR (1981) Truhlar DG (ed) Potential energy surfaces and dynamics calculations, Plenum, New York, pp 653–660
37. Steckler R, Truhlar DG (1990) J Chem Phys 93:6570
38. Heidrich D (1995) In: Heidrich D (ed) The reaction path in chemistry, Dordrecht, pp 1–10
39. Hoffman DK, Nord RS, Ruedenberg K (1986) Theor Chim Acta 69:265
40. Jørgensen P, Jensen HJA, Helgaker T (1988) Theor Chim Acta 73:55
41. Shida N, Almlöf JE, Barbara PF (1989) Theor Chim Acta 76:7
42. Quapp W (1989) Theor Chim Acta 75:447
43. Quapp W (1995) In: Heidrich D (ed) The reaction path in chemistry. Kluwer, Dordrecht pp 96–107; Quapp W, Imig O, Heidrich D (1995) In: Heidrich D (ed) The reaction path in chemistry. Kluwer, Dordrecht pp 130–160
44. Isaacson AD, Truhlar DG (1982) J Chem Phys 76:1380
45. Miller WH, Handy NC, Adams JE (1980) J Chem Phys 72:99
46. Lu Dh, Zhao M, Truhlar DG (1991) J Comput Chem 12:376
47. Lu Dh, Truhlar DG (1993) J Chem Phys 99:2723
48. Press WH, Teukolsky SA, Vetterling WT, Flannery BP (1992) In: Numerical recipes in FORTRAN, 2nd edn. Cambridge University Press, Cambridge (a) 413–417, (b) 57
49. Lu Dh, Truong TN, Melissas VS, Lynch GC, Liu Y-P, Garrett BC, Steckler R, Isaacson AD, Rai SN, Hancock GC, Lauderdale JG, Joseph T, Truhlar DG (1992) Comput Phys Commun 71:235
50. Steckler R, Hu W-P, Liu Y-P, Lynch GC, Garrett BC, Isaacson AD, Melissas V, Lu D-h, Truong TN, Rai SN, Hancock GC, Lauderdale JG, Joseph T, Truhlar DG (1995) Comput Phys Commun 88:341
51. Steckler R, Chuang Y-Y, Coitiño EL, Hu W-P, Liu Y-P, Lynch GC, Nguyen KA, Jackels CF, Gu MZ, Rossi L, Fast P, Clayton S, Melissas VS, Garrett BC, Isaacson AD, Truhlar DG (1996) POLYRATE, version 7.0, University of Minnesota, Minneapolis, Minn, (unpublished)
52. Walch SP, Dunning TH Jr (1980) J Chem Phys 72:1303; Schatz GC, Elgersma H (1980) Chem Phys Lett 73:21
53. Hehre WJ, Radom L, Schleyer PVR, Pople JA (1986) Ab initio molecular orbital theory. Wiley, New York
54. Gonzalez C, Schlegel HB (1990) J Phys Chem 94:5523
55. Chen Z (1989) Theor Chim Acta 75:481
56. Garrett BC, Truhlar DG, Grev RS, Magnuson AW (1980) J Phys Chem 84:1730; (1983) 87:4554(E)
57. Liu Y-P, Lynch GC, Truong TN, Lu D-h, Truhlar DG, Garrett BC (1993) J Am Chem Soc 115:2408
58. Truhlar DG, Kilpatrick NJ, Garrett BC (1983) J Chem Phys 78:2438
59. González-Lafont A, Truong TN, Truhlar DG (1991) J Chem Phys 95:8875
60. Melissas VS, Truhlar DG (1993) J Chem Phys 99:1013
61. Melissas VS, Truhlar DG (1994) J Phys Chem 98:875